NEOPLASIA
www.neoplasia.com
Volume 22 Number 11 November 2020 pp. 644–658

Loss of Fbxw7 triggers mammary tumorigenesis associated with E2F/c-Myc activation and Trp53 mutation

Alison E. Meyer [a]; Quinlan Furumo [a]; Cary Stelloh [a]; Alex C. Minella [a]; Sridhar Rao [a,b,*]

[a] Blood Research Institute, Versiti, 8727 Watertown Plank Rd., Milwaukee, WI 53226, USA;
[b] Departments of Cell Biology, Neurobiology, and Anatomy, and Pediatrics, Medical College of Wisconsin, 8701 Watertown Plank Rd., Milwaukee, WI 53226, USA

Abstract

Fbw7 is a tumor suppressor that regulates the degradation of oncogenic substrates such as c-Jun, c-Myc, Notch1 intracellular domain (ICD), and cyclin E by functioning as the substrate recognition protein in the Skp1-Cullin-F-box (SCF) ubiquitin ligase complex. Consequently, low expression or loss of *FBXW7* in breast cancer has been hypothesized to result in the accumulation of oncogenic transcription factors that are master regulators of proliferation, apoptosis, and ultimately transformation. Despite this, the direct effect of Fbw7 loss on mammary gland morphology and tumorigenesis has not been examined. Here, we demonstrate that conditional deletion of *Fbxw7* in murine mammary tissue initiates breast tumor development and also results in lactation and involution defects. Further, while *Fbxw7* loss results in the overexpression of Notch1-ICD, c-Jun, cyclin E, and c-Myc, the downstream transcription factor pathways associated with c-Myc and cyclin E are the most dysregulated, including at the single-cell level. These pathways are dysregulated early after *Fbxw7* loss, and their sustained loss results in tumorigenesis and reinforced c-Myc and cyclin E-E2F pathway disruption. We also find that loss of *Fbxw7* is linked to the acquisition of *Trp53* mutations, similar to the mutational spectrum observed in patients. Our results demonstrate that the loss of *Fbxw7* promotes the acquisition of *Trp53* mutations and that the two cooperate in breast tumor development. Targeting c-Myc, E2F, or p53 may therefore be a beneficial treatment strategy for *FBXW7*-altered breast cancer patients.

Neoplasia (2020) 22 644–658

Keywords: Fbw7, P53, Breast cancer, Tumor cell biology, Cell cycle

Introduction

Targeted degradation through the ubiquitin–proteasome system plays a critical role in the regulation of cell homeostasis, helping to constrain the enzymatic or transcriptional activity of substrate proteins to an appropriate time and location. Many proteins that are tightly controlled by ubiquitination are master regulators of proliferation, growth, apoptosis, and cell fate decisions, making the proteins involved in their degradation tumor suppressors. One such example is the evolutionarily conserved F-box protein Fbw7 (encoded by the gene *FBXW7*), which partners with Skp1 and Cullin1 to form the E3 ubiquitin ligase complex SCF^{Fbw7} [1]. Fbw7 is the substrate recognition subunit and binds proteins containing the canonical ``Cdc4 phosphodegron motif'' (CPD; 1). Binding enables the assembly of ubiquitin chains on the substrate, marking it for degradation. Targets of Fbw7 include the oncoproteins c-Myc, c-Jun, cyclin E, and Notch1-intracellular domain (Notch1-ICD; 1). Dysregulation of individual substrates can promote tumor development. For example, increased expression of cyclin E results in genomic instability, cell cycle dysregulation, mammary gland hyperplasia, and tumorigenesis [2–6]. Dysregulation of Fbw7 targets in other cancer types has also been observed [7–10], implying that Fbw7-mediated degradation is commonly altered during transformation. Additionally, point mutations in the CPD motif of some targets can occur [8,11,12], suggesting that the dysregulation of Fbw7 substrates in cancer may be widespread.

Alterations in either the expression level or mutational status of *FBXW7* have also been observed in multiple cancer types. While point mutations in *FBXW7* that disrupt substrate binding have been identified in some cancers, such mutations are found less often in breast cancer [13], where loss of *FBXW7* expression is much more common. Deletion of chromosome 4q31, which contains *FBXW7*, is seen in approximately 30% of primary breast cancers [9]. Gene silencing through *FBXW7* promoter methylation is also widely observed in breast cancer [14], and lower levels of *FBXW7* expression have been correlated with worse disease-free survival [9,15]. As such, loss of *FBXW7* may be a critical ``first-hit'' during

* Corresponding author at: Blood Research Institute, Versiti, 8727 Watertown Plank Rd., Milwaukee, WI 53226, USA.
e-mail addresses: AMeyer@Versiti.org (A.E. Meyer), QFurumo@Versiti.org (Q. Furumo), CStelloh@Versiti.org (C. Stelloh), aminella@me.com (A.C. Minella), sridhar.rao@versiti.org (S. Rao).

https://doi.org/10.1016/j.neo.2020.07.001

the development of breast cancer. Despite this evidence, the direct consequences of *FBXW7* expression loss on breast tumorigenesis have not been directly examined. While many studies have focused on the contribution of individual Fbw7 substrates to breast tumor development, the effects of *FBXW7* loss on substrate accumulation can vary significantly by tissue type. In an effort to identify the downstream consequences of reduced *Fbxw7* expression on mammary gland development and tumorigenesis, we utilized a Balb/c mammary mouse model of conditional *Fbxw7* loss. We find that *Fbxw7* loss triggers breast tumorigenesis that is associated with *Trp53* mutation and early/sustained upregulation of the E2F and c-Myc transcription factor pathways.

Materials and methods

Mice and genotyping

Animals were housed at the Medical College of Wisconsin. Procedures used were approved by the Institutional Animal Care and Use Committees at the Medical College of Wisconsin. Generation of the $Fbxw7^{flox/flox}$ mouse was published by Thompson et al. (2008) [16]. Mice were purchased from The Jackson Laboratory (Stock #017563). LGB-Cre mice are described by Selbert et al. (1998) [17] and were purchased from The Jackson Laboratory (Stock #017836). $Fbxw7^{flox/flox}$ mice were independently backcrossed six times to WT Balb/c mice (The Jackson Laboratory Stock #000651). To obtain $Fbxw7^{flox/flox}$;LGB-Cre+ females, $Fbxw7^{flox/flox}$ males were mated with LBG-Cre+ females. $Fbxw7^{flox/flox}$ mice were genotyped as described in Thompson et al. (2008) [16]. LGB-Cre positivity was genotyped with the primers F: 5′ GCC TGC ATT ACC GGT CGA TGC AAC GA 3′ and R: 5′ GTG GCA GAT GGC GCG GCA ACA CCA TT 3′. Excision of *Fbxw7* exons 5 and 6 in $Fbxw7^{flox/flox}$; LGB-Cre+ tissues was assayed by PCR as described in Thompson et al. (2008) [16]. Survival was calculated using GraphPad Prism v. 8.0.1.

Immunohistochemistry

Tissue sections were deparaffinized in xylene for 2 × 10 min each followed by 100, 90, and 70% ethanol solutions for 10 min each. Sections were rinsed in water for 5 min and boiled for 20 min in 10 mM citric acid, pH 6.0. After cooling (15 min), sections were placed in 3% H_2O_2 in methanol in the dark for 20 min. Tissues were rinsed in PBS for 5 min and then blocked in 10% normal goat serum in PBS-0.025% Triton X-100 for 1hr. Sections were washed in water for 2 min and then blocked using the Avidin/Biotin blocking kit (Vector Laboratories, SP-2001). Tissues were stained overnight in 10% NGS, PBS-0.025% Triton X-100 with the following antibodies and dilutions: Fbw7 1:200 (gift of Bruce E. Clurman and described in [18], Ki67 1:200 (Abcam, ab15580), Cleaved caspase 3 1:200 (Cell Signaling Technologies, 9661S), c-Myc 1:100 (Abcam, ab32072), cyclin E 1:200 (Sigma, HPA018169), Notch1 1:50 (Cell Signaling Technologies, 3268S), c-Jun 1:100 (Abcam, ab32137), β-casein 1:100 (Santa Cruz, sc-166684), p53 1:200 (2524S), ERα 1:100 (EMD-Millipore, 06-935), and PR 1:100 (Abcam ab16661). After 3 × 5 min washes in PBS-0.025% Triton X-100, samples were processed using the Vectastain rabbit or mouse peroxidase IgG kits (Vector Laboratories, PK-4001 and PK-4002) and visualized with DAB reagent (Vector Laboratories, SK-4100). After washing in PBS, samples were stained with hematoxylin (Sigma, MHS16-500ML) and dehydrated in 70, 90, and 100% ethanol washes for 5 min each followed by 2 × 5 min xylene washes. Sections were mounted and imaged using a Nikon Eclipse 50i scope equipped with a Nikon Digital Sight DS-L3 camera.

Isolation of mammary epithelial single cells

Following euthanasia, all mammary glands were removed and minced into a fine paste with razors. The tissue was weighed and placed into collagenase solution (0.2% trypsin, 0.2% collagenase A, 5% FBS, 5 μg/mL gentamycin in DMEM/F12). 10 mL of collagenase solution was used for each gram of tissue. Tissue was digested with shaking at 37 °C for 2 h, with pipetting every 30 min. Digested tissue was centrifuged at 1500 rpm for 5 min, and the pellet was resuspended in 10 mL serum free DMEM/F12. To reduce the number of fibroblasts, the mixture was pulse-spun at 500 g for 7 s and the supernatant was removed. This was repeated 5–8 times until the supernatant appeared clear. The pellet was resuspended in 5 mL of red cell lysis buffer (Sigma, R7757), placed in a clean 15 mL conical tube, and incubated for 5 min. After a 5 min spin at 500 g, the pellet was resuspended in serum free DMEM/F12 and centrifuged. The pellet was resuspended in 2 mL 0.25% Trypsin-EDTA with 10 μL of DNAse and transferred to a 6 cm dish. Cells were pipetted rigorously for 5 min or until a complete dissociation of organoids into single cells was observed under a microscope. 5 mL of DMEM/F12 with 10% FBS was added, and cells were filtered through a 40 μM cell strainer twice. Cells were centrifuged at 200g for 5 min, and resuspended in 3–6 mL of DMEM/F12 with 10% FBS. Epithelial enrichment was performed using the EasySep Mouse Epithelial Cell Enrichment Kit (Stemcell Technologies, 13309).

Single cell qPCR

Single cell qPCR was performed using the Fluidigm C1/BiomarkHD systems. 5–10 μm pre-amp IFCs were used to isolate single cells and for subsequent cDNA generation. Cells were loaded at a concentration of 200,000 cells/mL and were visualized with a Nikon EVOS microscope. Dead cells or chambers containing more than one cell were excluded. cDNA was prepared according to the Preamplification Using Delta Gene Assays guide (available on Fluidigm's website). Delta gene assays for c-Myc, E2F, c-Jun, and Notch-ICD targets were purchased from Fluidigm (See Supplementary Table 1 for details) to measure mRNA levels, and RNA spike controls were included for normalization of expression (ArrayControl RNA Spikes, ThermoFisher Scientific, AM1780). qPCR was performed on a 96.96 Dynamic Array using the BiomarkHD system. Data were analyzed using the Fluidigm Real-Time PCR Analysis software. Data points for each gene (single cell values) lacking amplification or with poor melt curves were removed. Ct values were normalized to RNA spike controls and subtracted from the limit of detection (Ct of 24). Final values are expressed as Log_2Expression. Differences between groups were analyzed using GraphPad Prism v. 8.0.1 and the Mann-Whitney U test using a p value cutoff of <0.05. See Supplementary Tables 2–5 for all single cell qPCR data.

RNA sequencing

For epithelial RNA isolation, cells were resuspended in 1 mL Trizol (ThermoFisher Scientific, 15596018). RNA was isolated according to the manufacturer's recommended protocol. RNA quality was measured by NanoDrop 2000 (ThermoFisher Scientific) and on an Agilent 2200 TapeStation analyzer. RNA samples of lower quality (260/280 <1.9 or RIN value <7) were further purified using the RNeasy Plus kit (Qiagen, 74134). For mammary gland and tumor samples, tissues were homogenized in Trizol and similarly processed.

For RNA sequencing, ERCC Spike-In Mix (ThermoFisher Scientific, 4456840) was added. Libraries were prepped in accordance with the NEBNext Ultra II RNA library prep kit (New England Biolabs, E7770) in combination with the NEBNext Poly(A) mRNA magnetic isolation

module (New England Biolabs, E7490), the NEBNext multiplex oligos set 1 (New England Biolabs, E7335), and Ampure XP magnetic beads (Beckman Coulter, A6388). Libraries were quantified using the NEBNext library quant kit (New England Biolabs, E7630) and combined with PhiX control v3 (Illumina, 15017666). Pooled libraries were run on an Illumina NextSeq 500 system using paired end sequencing (38 × 2).

Raw RNA sequence reads were mapped to mouse reference genome mm9 using Salmon (v1.2.0) and default parameters, and were normalized using ERCC spike-ins. Differential Expression analysis was done using the DESeq2 (v1.24.0) package in R. Differentially expressed genes were identified as significant at a Benjamini-Hochberg adjusted p-value <0.05 and an absolute fold change of 2 (|Log2FC|>1). Heatmaps were done in R using pheatmap (v1.0.12) with the Euclidean method for distance and k-means clustering. The MMTV-PyMT 8 week tumor time point RNA sequencing data published by Cai et al. (2017) [19] were downloaded from GEO Omnibus (Accession number GSE76772). We analyzed GSM2037468, GSM2037476, and GSM2037484, which represent 3 replicates of the 8 week time point. DESeq analysis comparing our expression data with those of Cai et al. (2017) [19] was performed as described above.

For GSEA, gene expression data for each condition alongside a mouse to human gene symbol conversion file were loaded into GSEA 4.0.3 (Broad Institute). The human derived cancer (h.all.v7.0) dataset was queried using 1000 as the set number of permutations, and permutation type was set to gene_set. Only those genesets that met the false discovery rate of 0.25 and NOM $p < 0.01$ were considered.

Analysis of Trp53 mutations

Genomic DNA was isolated from tissue samples in 75 µL of 25 mM NaOH/0.2 mM EDTA for 1 h at 98 °C. After cooling to room temperature, 75 µL of 40 mM Tris HCl (pH 5.5) was added to neutralize the

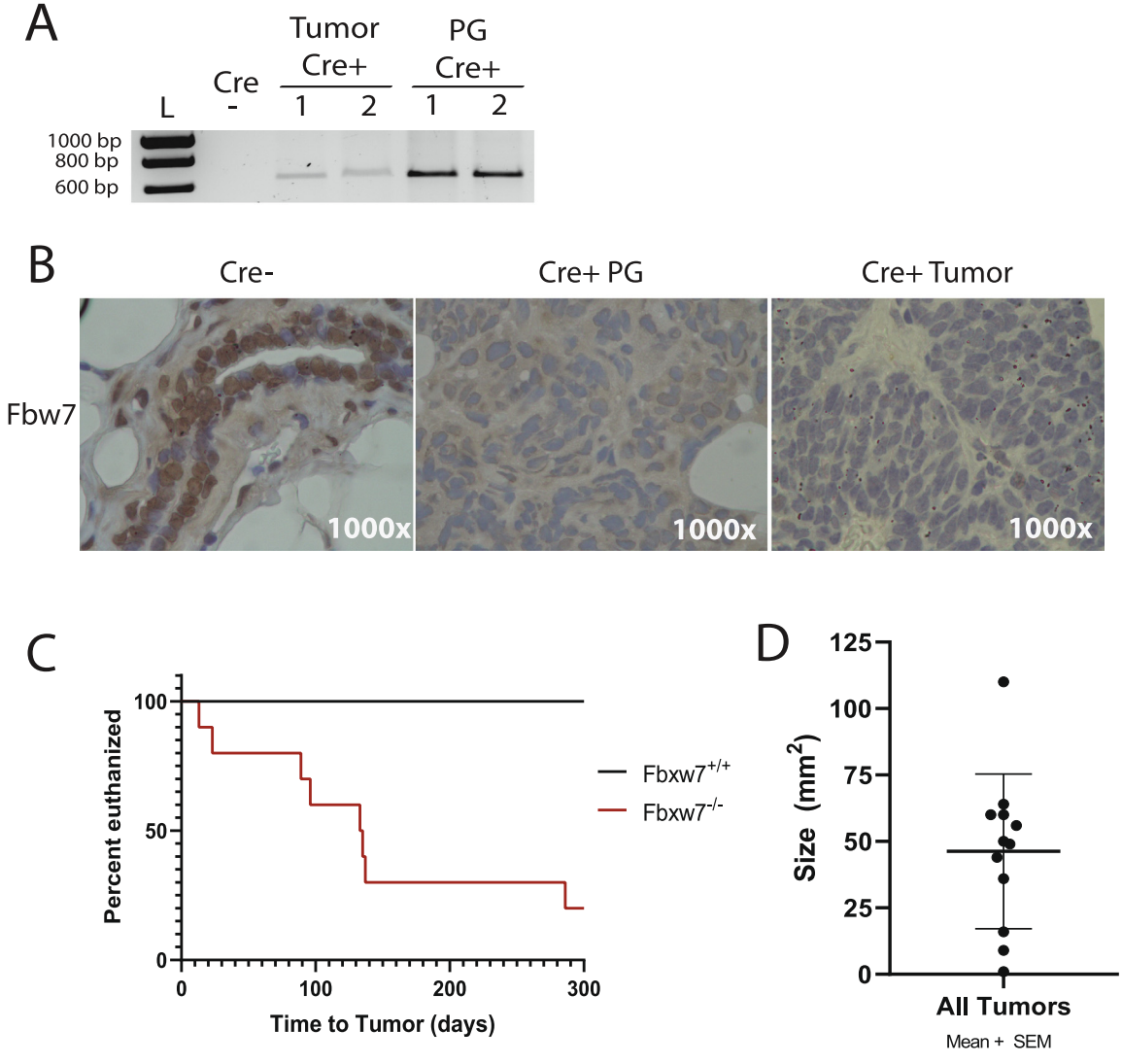

Fig. 1. *Fbxw7* loss triggers mammary tumorigenesis. A. PCR analysis for excision of exons 5–6 in murine *Fbxw7* was performed on DNA extracted from control (Cre-) mammary tissue, tumor samples from Cre+ mice, and mammary glands from Cre+ mice in their third week of pregnancy. Proper excision results in a band of ~650 bp. Representative results shown from 1 control (Cre-), 2 tumors (Tumor Cre+ 1 and 2), and 2 pregnant Cre+ mice (PG Cre+ 1 and 2). L = molecular weight ladder. B. IHC for Fbw7 showing expression in control Cre- tissue and loss of expression in one example Cre+ PG animal and one example Cre+ tumor. Magnification = 1000×. C. Mice were sacrificed at the time of tumor discovery, and the time to tumor for each animal is shown. D. The size (area) of each tumor was measured at the time of sacrifice and the mean size + SEM was plotted. Note that 8/10 mice developed tumors, with 4 developing more than 1 tumor, thus $N = 12$.

samples. After centrifugation, 2 μL of resulting DNA was used in PCR amplification of exons 5–6 or 7–8 using LongAmp Taq mastermix (New England Biolabs, M0287S) and the following primers:

Exons 5–6: 5′-CGTTACTCGGCTTGTCCCCGACCT-3′and 5′-CAACTGTCTCTAAGACGCACAAC-3′
Exons 7–8: 5′-GAGGTAGGGAGCGACTTCACCTGG-3′and 5′-TGAAGCTCAACAGG CTCCTCCGCCTCC-3′

Amplicons were cloned using the TA Cloning Kit (Invitrogen/ThermoFisher, K204001). To determine mutations in *Fbxw7*$^{-/-}$ cells or tumors, comparisons were made with WT tail samples taken from the same mouse as the cells or tumor.

Results

Fbxw7 loss initiates mammary tumor development

To determine if loss of *Fbxw7* would initiate the development of breast tumors, we modified a published mouse model of inducible *Fbxw7* gene excision previously used to study hematopoiesis [16]. In this model, exons 5 and 6 in both alleles of *Fbxw7* are flanked by LoxP sites (*Fbxw7*$^{fl/fl}$). Thompson et al. [16] previously showed that Cre-mediated excision of exons 5 and 6 results in a complete loss of Fbw7 protein expression. To direct *Fbxw7* excision specifically within the mammary gland, we mated *Fbxw7*$^{fl/fl}$ mice with beta-lactoglobulin (LGB)-Cre transgenic mice [17]. The LGB promoter drives Cre expression in the mammary gland epithelial cells during pregnancy and subsequent lactation, and thus *Fbxw7* excision in the breast epithelium is inducible by pregnancy. We examined the effect of *Fbxw7* loss in 10 *Fbxw7*$^{fl/fl}$;LGB Cre+ and 8 control *Fbxw7*$^{fl/fl}$;LGB Cre- animals. Excision of *Fbxw7* in Cre+ animals was verified in any tumors that developed and in nearby healthy mammary glands using PCR primers specific to the excised allele (representative results shown in Fig. 1A; [16]). While excision was observed following the first pregnancy (Fig. 1A, PG Cre+ lanes), the majority of animals underwent two pregnancies. Loss of Fbw7 protein expression in the mammary glands of pregnant Cre+ mice and any resulting tumors was verified by IHC (representative tissues shown in Fig. 1B). These data indicate that *Fbxw7* expression is lost upon pregnancy in the mammary glands of *Fbxw7*$^{fl/fl}$;LGB Cre + mice.

We next determined whether *Fbxw7* loss promotes breast tumor development. Beginning at the time of first pregnancy, all animals were palpated weekly to identify tumors. As our goal was to establish if *Fbxw7* loss alone would promote tumor development, and multiple genetic hits or the use of immunocompromised mice are typically required to observe metastasis in breast cancer models [20–22], identification of palpable tumors was defined as the experimental endpoint. No tumors were noted in any of the *Fbxw7*$^{+/+}$ control mice. In contrast, 8/10 (80%) of *Fbxw7*$^{-/-}$

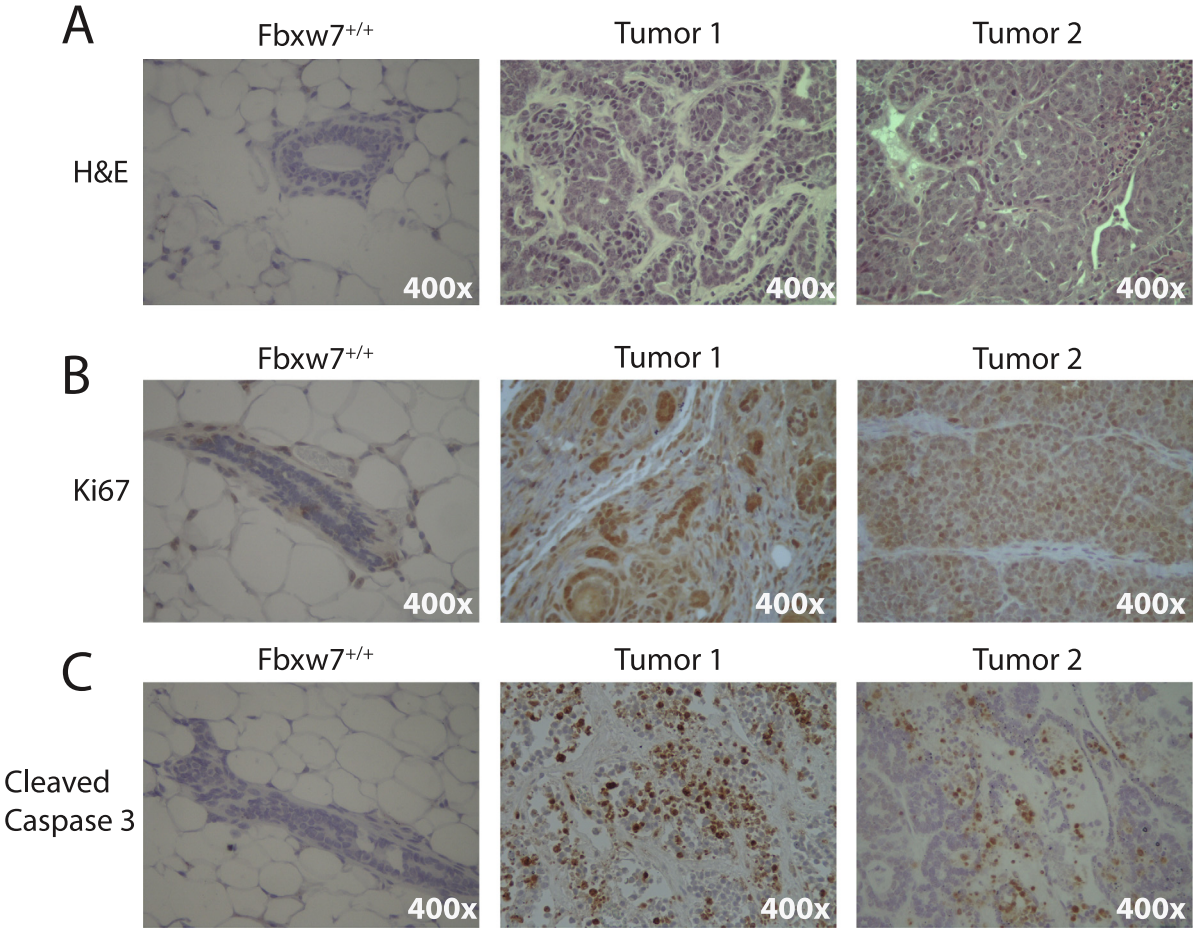

Fig. 2. *Fbxw7*$^{-/-}$ tumors are highly proliferative and apoptotic. A. Representative results of H&E staining showing normal breast architecture in a control *Fbxw7*$^{+/+}$ animal and excessive filling of the fat pad and epithelial proliferation in two independent *Fbxw7*$^{-/-}$ tumors. B. Representative IHC results showing Ki67 staining (marking proliferation), which is low in control tissues and high in tumors. C. Representative IHC results for cleaved caspase 3 marking increased apoptosis in tumors. Little apoptosis was observed in control animals. All images 400×.

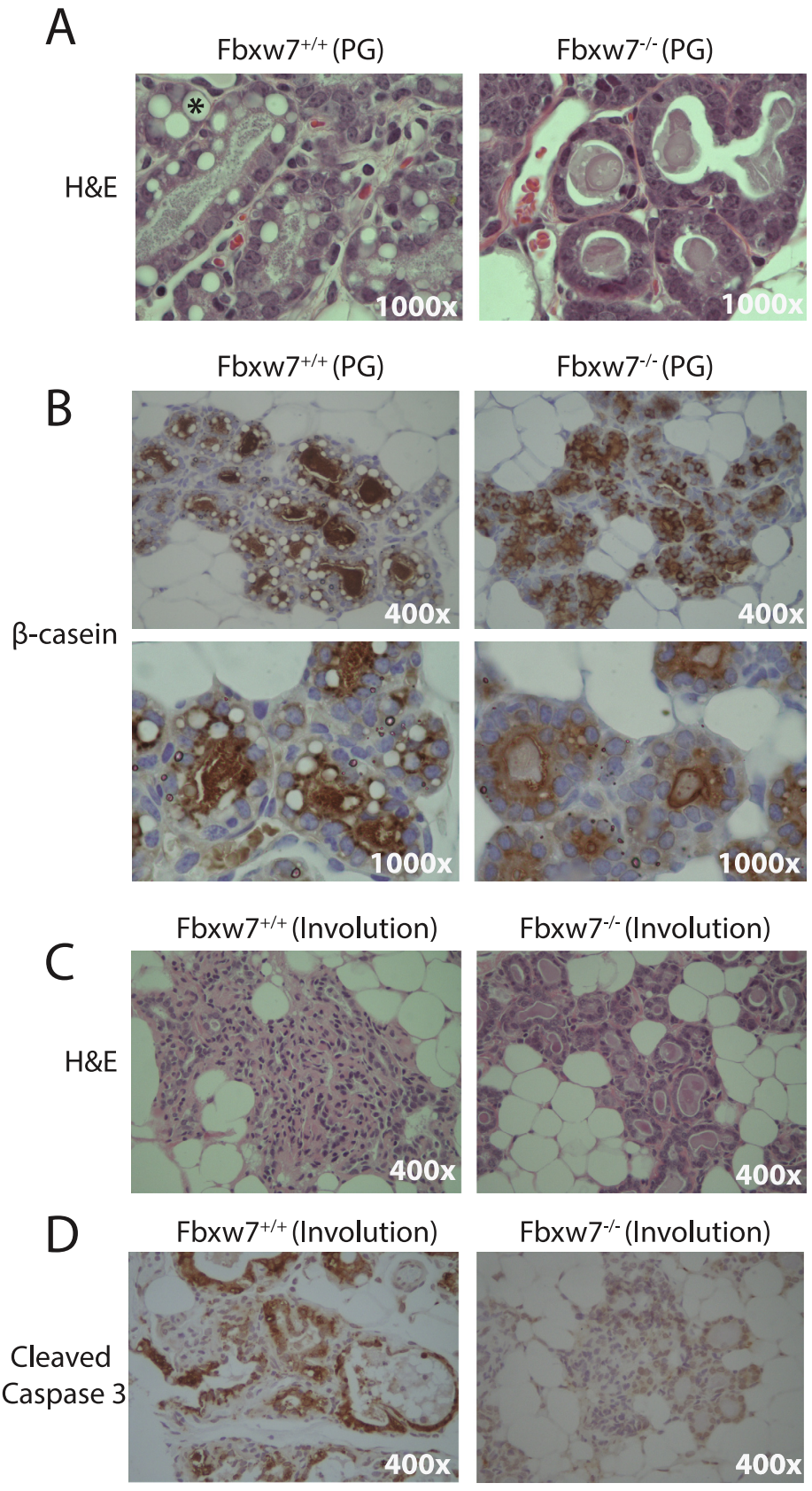

Fig. 3. *Fbxw7* loss results in lactation deficiency and disrupted involution. A. H&E staining from representative control $Fbxw7^{+/+}$ as well as $Fbxw7^{-/-}$ mammary tissues. Tissue sections were taken from mice during the third week of pregnancy. $Fbxw7^{-/-}$ mice show a lack of lipid droplets (marked with * in $Fbxw7^{+/+}$ panel) and a less granular staining in the lumina than $Fbxw7^{+/+}$ mice. Images taken at 1000×. B. IHC for β-casein shows a reduction in $Fbxw7^{-/-}$ versus $Fbxw7^{+/+}$ lumina. Upper panel = 400×, lower panel = 1000×. C. H&E staining of mammary tissue from representative $Fbxw7^{+/+}$ and $Fbxw7^{-/-}$ mice 5 days into involution. Images taken at 400×. D. IHC staining for cleaved caspase 3 showing weaker staining in the $Fbxw7^{-/-}$ glands at 5 days involution vs. control glands. Images 400×.

animals developed palpable tumors, with the time to tumor detection from the date of the first pregnancy ranging from 13 to 286 days (Fig. 1C). 3/10 mice developed tumors after a single pregnancy, with an additional 5/10 undergoing a second pregnancy prior to tumor development. Four mice had tumors identified simultaneously in distinct locations. Mice were sacrificed upon tumor palpation and the area of each tumor was measured following excision to obtain a more accurate size measurement, as localized swelling or other factors may contribute to the palpable mass size. Tumor size ranged from 1 mm^2 for the smallest to 110 mm^2 for the largest, with an average tumor size of ~46.3 mm^2 (Fig. 1D). Tumor location was variable, with tumors found in thoracic, abdominal, and inguinal mammary glands. No additional non-palpable tumors were observed following dissection, with no gross evidence of metastatic disease in the lungs or livers (data not shown). As the longest time to tumor from first pregnancy was 286 days (~40 weeks), the two remaining *Fbxw7*$^{-/-}$ animals and all control animals were aged to 40 weeks post primary pregnancy before sacrifice. No mammary tumors were observed in these animals upon dissection. 1/8 control animals developed a large intestine mass which was not positive for *Fbxw7* excision and deemed an unrelated tumor. By H&E, large areas of epithelial cell hyper-proliferation were noted in the tumors, with excessive filling of the fat pad (Fig. 2A). Tumors were moderately- to well-differentiated, as evidenced by the presence of retained normal breast architecture or collapsed/filled-in tubules. No local invasion of tumors into the surrounding muscle tissue was noted in any of the specimens, consistent with their relatively well-differentiated appearance by histology. Consistent with hyper-proliferation, prevalent staining of the proliferation marker Ki67 was observed in the tumors (Fig. 2B). Areas of apoptosis were also observable, as indicated by cleaved caspase 3 staining (Fig. 2C). We also examined estrogen receptor (ERα) and progesterone receptor (PR) status by IHC (Supplementary Fig. 1). While some intra-tumor heterogeneity was observed, the majority of tumors were ERα-positive and PR negative (Supplementary Fig. 1). The phenotype of ERα+, PR-, and high Ki67 staining is most consistent with a luminal B-like subtype. We conclude that loss of *Fbxw7* expression promotes

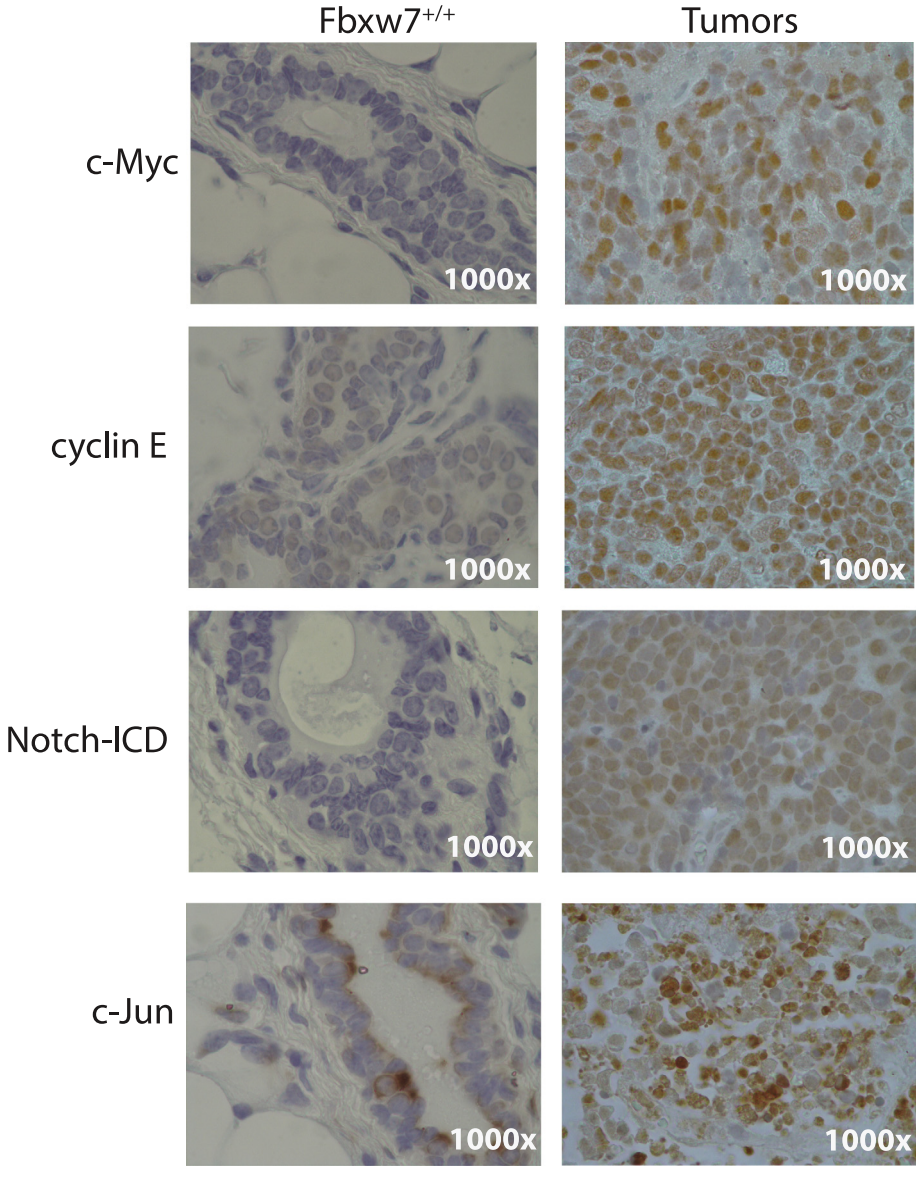

Fig. 4. Oncogenic substrates of Fbw7 are overexpressed in *Fbxw7*$^{-/-}$ mammary glands. IHC was performed on mammary tissue sections from control *Fbxw7*$^{+/+}$ animals vs. *Fbxw7*$^{-/-}$ tumors. Representative results are shown. Increased staining for c-Myc, cyclin E, Notch1-ICD, and c-Jun was observed in tumor tissues vs. control. All images 1000×.

mammary tumor development and results in increased proliferation and apoptosis.

Fbxw7$^{-/-}$ mice exhibit impaired lactation and involution

All mice were able to carry their litters to term, and no differences in litter size were observed. Importantly, the *Fbxw7*$^{-/-}$ mice were unable to nurse their pups long-term. All pups born from *Fbxw7*$^{-/-}$ mothers died between 1 and 7 days of age. However, pups were successfully nursed by WT foster mothers, indicating *Fbxw7*$^{-/-}$ mothers have a lactation defect. This phenotype is similar to that reported by Hu et al. in mice overexpressing the Fbw7 target *Notch1* [23]. Defects in lactation have also been observed upon c-Myc overexpression [24].

To better delineate the observed lactation defect in *Fbxw7*$^{-/-}$ mothers, we examined mammary gland development in virgin mice, during late pregnancy, and 5 days post involution. No differences were observed in the mammary glands in virgin mice (data not shown), which was expected due to intact *Fbxw7* alleles in both Cre- and Cre+ mice. In contrast, changes were readily observed in pregnant *Fbxw7*$^{+/+}$ vs. *Fbxw7*$^{-/-}$ mice. Although no differences in alveolar or lobular size was noted, glands in *Fbxw7*$^{-/-}$ pregnant mice contained fewer lipid droplets (Fig. 3A). Milk secretions were observable in the lumina in both genotypes, however the staining was more granular in the *Fbxw7*$^{+/+}$ animals, indicating differences in milk composition between the two genotypes (Fig. 3A). We next performed IHC for the milk protein β-casein and observed abnormal staining in the *Fbxw7*$^{-/-}$ alveoli. Although β -casein was readily detectable, higher magnification revealed little β -casein accumulation in the lumina of *Fbxw7*$^{-/-}$ mice compared to *Fbxw7*$^{+/+}$ mice (Fig. 3B). These data suggest that *Fbxw7*$^{-/-}$ mice are unable to nurse their litters due to defects in milk composition and secretion.

In addition to lactation defects, dysregulation of the Fbw7 targets Notch-ICD, c-Myc, and cyclin E have been associated with aberrant

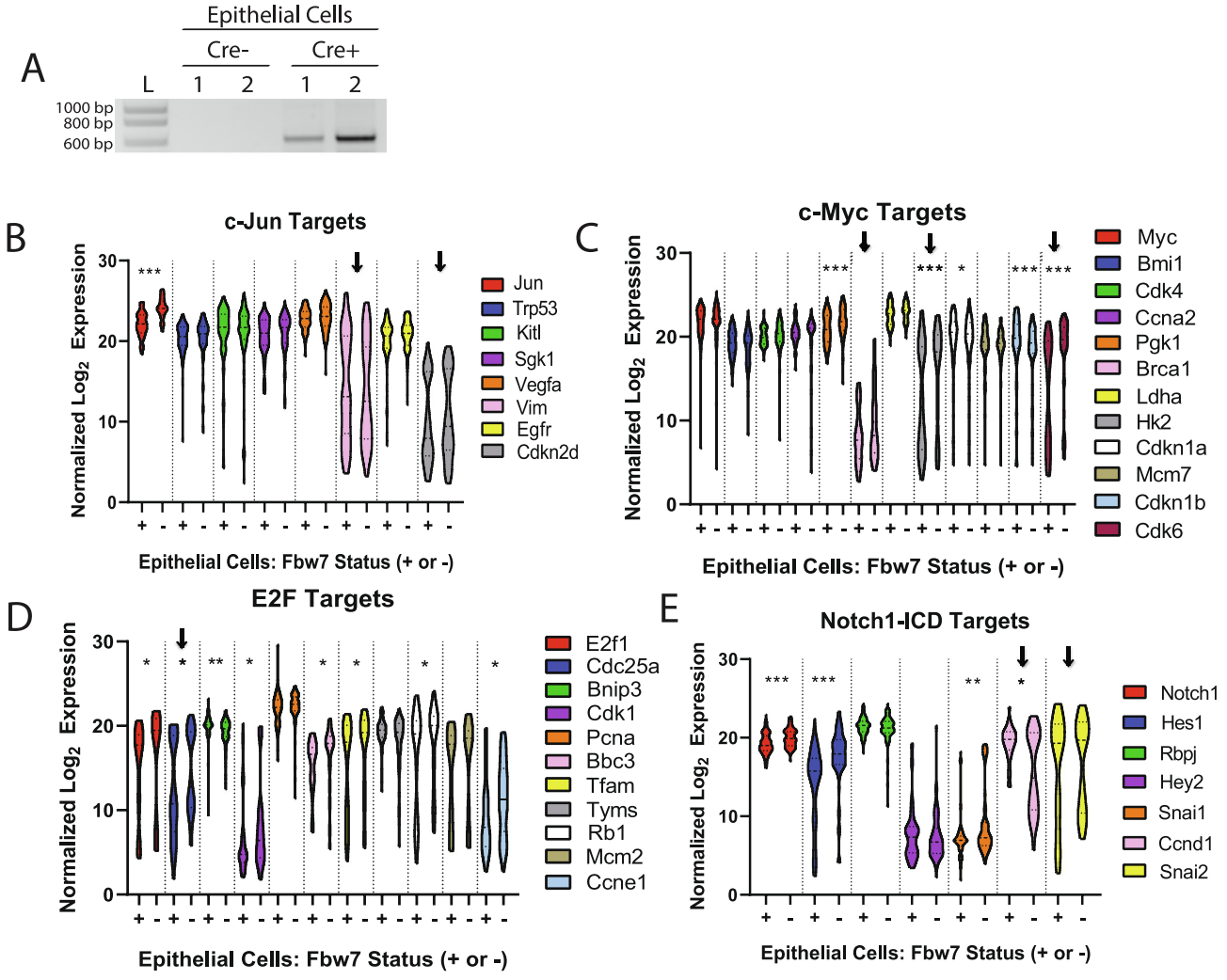

Fig. 5. Early loss of *Fbxw7* results in dysregulated c-Myc, E2F, and Notch-ICD target expression. A. Mammary epithelial cells were isolated from two control (Cre-) and two *Fbxw7*$^{-/-}$ (Cre+) mice during the third week of pregnancy. PCR analysis for the excision of exons 5–6 of *Fbxw7* was performed as in Fig. 1A. L = molecular weight ladder. B-E. Single cells were isolated from the populations shown in A using the Fluidigm C1 system and qPCR assays were performed using a Biomark HD (Fluidigm). Target amplification was performed with Delta Gene assays (primer sets) from Fluidigm for (B) c-Jun, (C) c-Myc, (D) E2F, and (E) Notch1-ICD target genes of interest. Lanes marked with + indicate *Fbxw7*$^{+/+}$ control cells and lanes marked with - indicate *Fbxw7*$^{-/-}$ cells. Statistical analysis was performed using the Fluidigm Real-Time PCR Analysis software. Data are expressed as Log_2Expression normalized to RNA spike-in controls. Significance was measured using the Mann-Whitney test with a p value cutoff of $p < 0.05$. *$p < 0.05$, **$p < 0.01$, ***$p < 0.001$. Arrows indicate genes exhibiting a distinct bimodal distribution. See Supplementary Tables 2–5 for data included in these analyses.

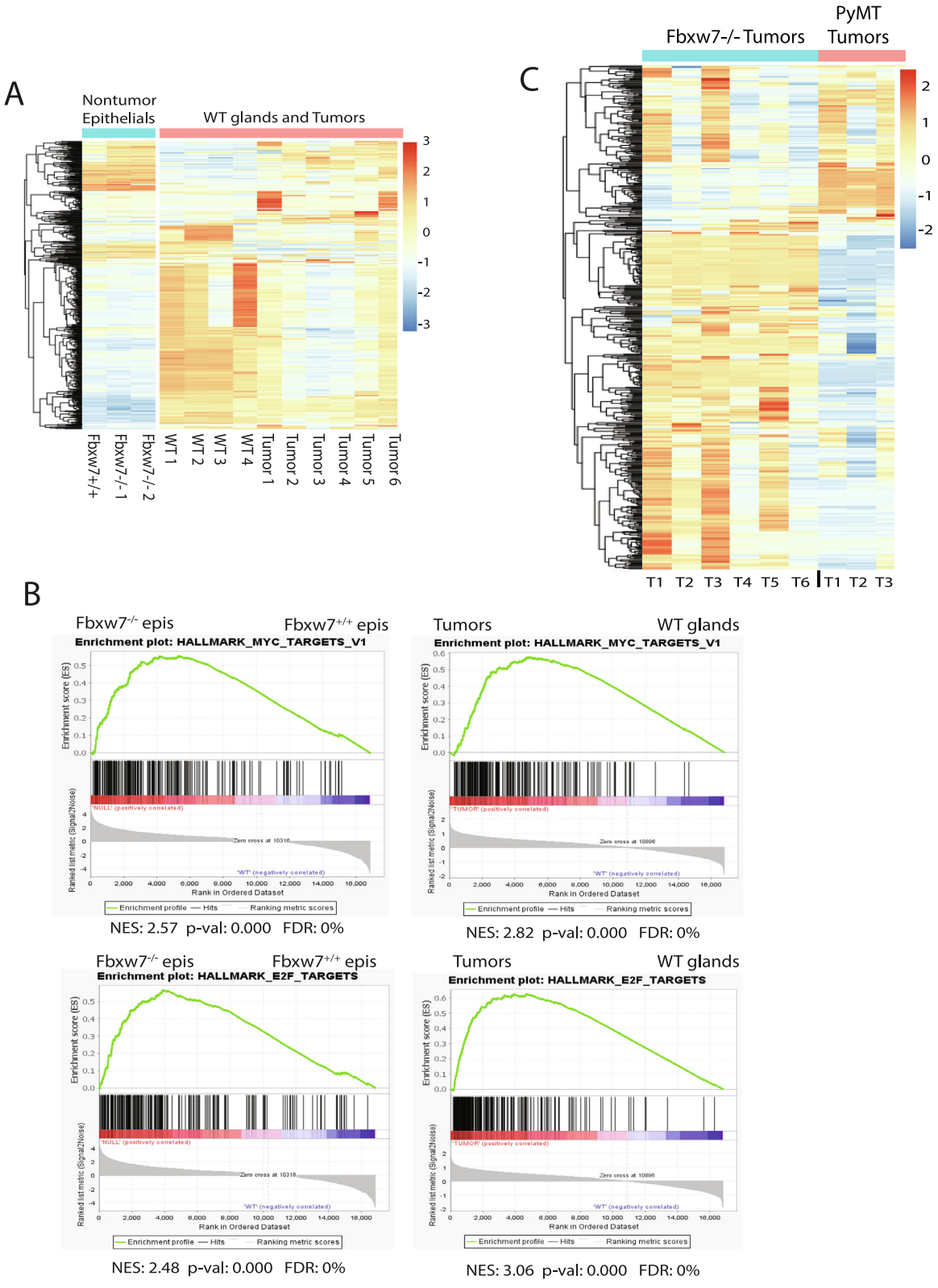

Fig. 6. *Fbxw7* loss results in E2F and c-Myc pathway dysregulation. A. Heatmap showing significantly differentially expressed genes (2-fold change, *p*-val adj <0.05) in non-tumor *Fbxw7*$^{+/+}$ and *Fbxw7*$^{-/-}$ epithelial cells (left, blue bar) and WT mammary tissue vs. *Fbxw7*$^{-/-}$ tumors (right, pink bar). B. Left panels: GSEA analysis was performed on bulk RNA sequencing data from non-tumor epithelial (epis) cells. Genesets that were enriched in the *Fbxw7*$^{-/-}$ vs. *Fbxw7*$^{+/+}$ cells included c-Myc (top) and E2F (bottom) targets. Only those genesets that met the cutoff of $p < 0.01$ and an FDR of < 25% were considered. Right panels: GSEA was performed on bulk RNA sequencing data from WT mammary tissue vs. tumors. Similar genesets were enriched in the tumor samples as in the *Fbxw7*$^{-/-}$ nontumor epithelial cells, however the normalized enrichment scores (NES) increased for c-Myc (top) and E2F (bottom) targets. C. Heatmap showing significantly differentially expressed genes (2-fold change, *p*-val adj <0.05) in *Fbxw7*$^{-/-}$ tumors (left, blue bar) vs. MMTV-PyMT 8 week tumors from Cai et al. (2017) (right, pink bar; 19).

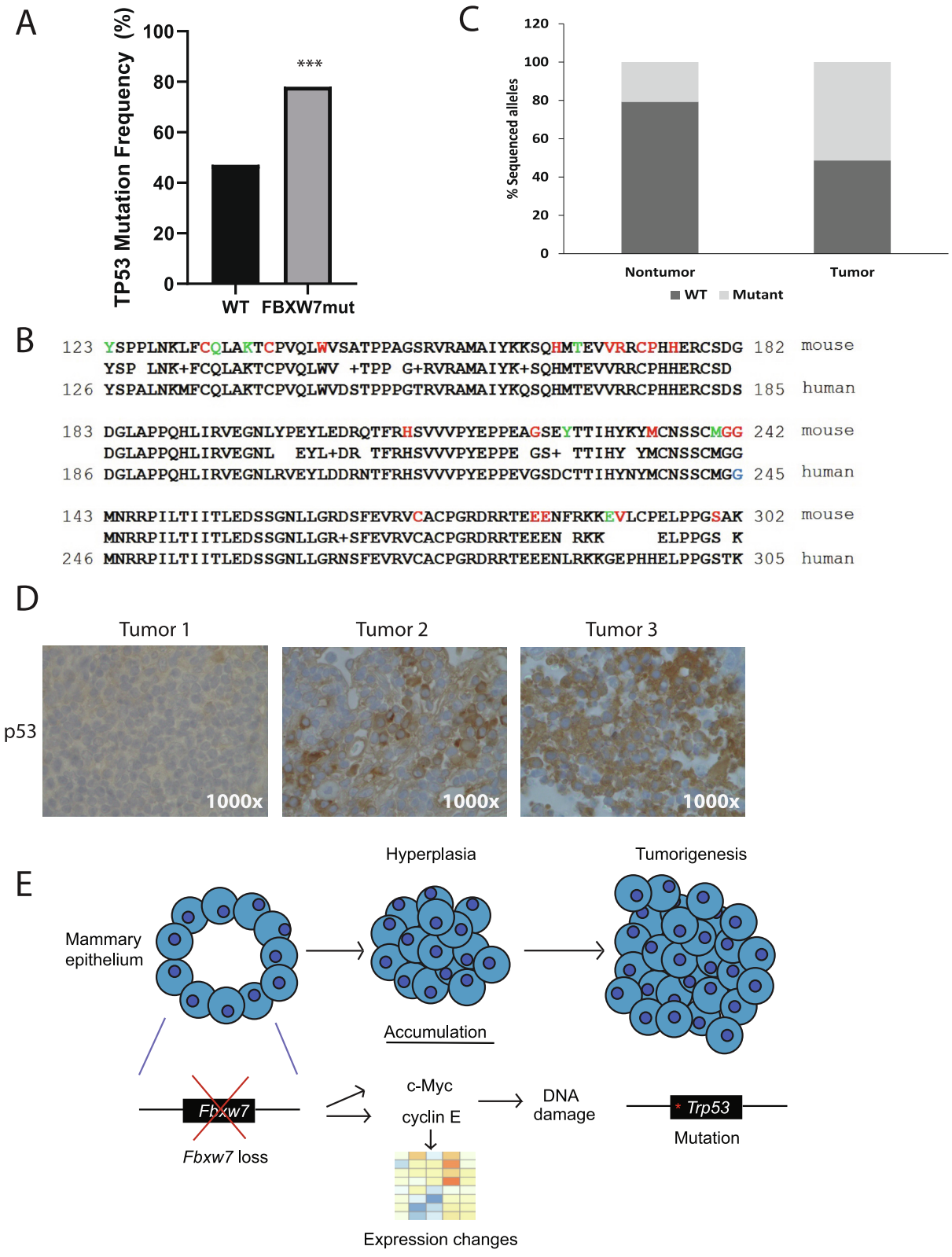

Fig. 7. *Fbxw7* loss results in *Trp53* mutation. A. cBioPortal was used to query datasets encompassing 8874 breast cancer patients across 15 studies for *FBXW7* and *TP53* mutational status. Patients that harbored a *FBXW7* mutation had an increased frequency of *TP53* mutations compared to *FBXW7* WT patients. ***$p < 0.001$, one-sided Fisher's exact test. B. Alignment of the mouse and human *TP53* gene sequences, with all identified mutations in the nontumor samples highlighted in green and those in the tumor samples in red. The blue reside (G245) in the human sequence indicates a ``hotspot'' mutation in human breast cancer. C. Graph depicting percentage of sequenced alleles that were mutated vs. nontumor (left) and tumor (right) samples. D. IHC for p53 in three separate tumor samples, with tumors 2 and 3 showing elevated expression and partial nuclear exclusion of p53. All photos 1000×. E. Model for breast tumorigenesis triggered by *Fbxw7* loss. *Fbxw7* depletion results in upregulation of Notch-ICD, c-Myc, and cyclin E, which impact cell cycle, DNA damage response, and G2/M checkpoint genes. Enforced proliferation in the presence of DNA damage provides a selective pressure for the acquisition of *Trp53* mutations, facilitating transformation.

involution. As defects were reported as early as 5 days post-weaning in these studies [23–25], we examined the mammary glands of *Fbxw7*$^{+/+}$ and *Fbxw7*$^{-/-}$ mice at this time point. Weaning occurred at 3 weeks post-partum for *Fbxw7*$^{+/+}$ mice and was defined as 3 weeks post-partum for *Fbxw7*$^{-/-}$ mice due to their inability to nurse. Five days following this time point, acinar collapse was observable in the *Fbxw7*$^{+/+}$ animals, indicating normal involution (Fig. 3C). In contrast, the 5 day post-involution glands from *Fbxw7*$^{-/-}$ mice were indistinguishable from pregnant glands, with no observable alveolar collapse (Fig. 3C). As involution requires apoptosis, we performed IHC for cleaved caspase 3, and found weaker staining in the *Fbxw7*$^{-/-}$ animals compared to the *Fbxw7*$^{+/+}$ controls (Fig. 3D). Collectively, these data indicate that *Fbxw7* loss results in both lactation and involution defects, similar to what has been reported with dysregulation of the Fbw7 substrates Notch1-ICD, cyclin E, and c-Myc.

Substrate proteins and their downstream transcriptional targets are dysregulated following loss of Fbxw7

Fbw7 loss can result in differential accumulation of substrate proteins depending on tissue type. We hypothesized that transformation following loss of *Fbxw7* may be due to the accumulation of substrates with critical roles in mammary gland morphogenesis and tumor biology such as c-Myc, cyclin E, Notch1-ICD, and c-Jun. First, we performed IHC on tumor and control mammary sections for c-Myc, cyclin E, c-Jun and Notch1-ICD. Staining for all four substrates was strongly observed in tumor sections, with minimal staining in corresponding control mammary gland sections (Fig. 4). These data suggest that multiple substrate proteins accumulate in the mammary tumors that develop upon *Fbxw7* loss, consistent with decreased Fbw7-mediated degradation. The overexpression of cyclin E, c-Myc, and Notch1-ICD is also consistent with the observed effects of *Fbxw7* loss on lactation and involution [23–25] and suggests that loss of *Fbxw7* broadly disrupts normal mammary development and function and promotes tumorigenesis through the sustained dysregulation of key substrates.

c-Myc, Notch1-ICD, and c-Jun are transcription factors that control the expression of many genes involved in tumor development. Additionally, active cyclin E-Cdk2 and c-Myc can induce the activation or expression of the E2F transcription factor family, particularly E2F1 and E2F3A, which are activated in late G1 and S phases and overexpressed in breast cancer [26–28]. As we observed a strong accumulation of c-Myc, Notch1-ICD, c-Jun, and cyclin E in our tumor tissues, we hypothesized that dysregulation of these substrates and associated transcription factor pathways may be a critical driver of tumor development. Further, we hypothesized that such dysregulation would occur early after *Fbxw7* loss. To address this hypothesis, we performed single cell qPCR analysis on non-cancerous, purified mammary epithelial cells isolated from two control *Fbxw7*$^{fl/fl}$;LGB Cre- and two *Fbxw7*$^{fl/fl}$;LGB Cre+ mice during late pregnancy. *Fbxw7* gene excision was verified in the isolated Cre+ cells (Fig. 5A). For qPCR, we assayed published downstream targets for c-Myc (12 genes), E2F (11 genes), Notch1-ICD (7 genes), and c-Jun (8 genes; References provided in Supplementary Table 1) using the Fluidigm C1 and Biomark HD platforms. The values obtained for each cell and gene shown in Fig. 5 are provided in Supplementary Tables 2–5. With the exception of c-Myc, mRNA levels of the transcription factors themselves were increased early after *Fbxw7* loss (Fig. 5B-E). Surprisingly, of the c-Jun targets we assayed, only *Jun* itself was significantly affected by *Fbxw7* loss (Fig. 5B).

We observed statistically significant changes in the expression of 5/12c-Myc targets in *Fbxw7* null cells (Fig. 5C). These genes were upregulated with the exception of *Cdkn1b* (encoding the cyclin/Cdk inhibitor p27), which is known to be repressed by c-Myc [26]. These data are consistent with c-Myc transcription factor activity following *Fbxw7* loss. The majority of the E2F targets we examined (8/11) were also affected by *Fbxw7* loss (Fig. 5D). These 8 genes are known to be upregulated by E2F (see Supplementary Table 1), and most were observed to be upregulated in our *Fbxw7* knockout cells. With regard to Notch1-ICD, we observed dysregulation of 4/7 targets in the *Fbxw7* null cells (Fig. 5E). Along with *Notch1* itself, we found that *Hes1* and *Snai1* were, as expected, upregulated following *Fbxw7* loss. However, *Ccnd1* is reported to be upregulated by Notch1-ICD, and we instead saw a downregulation of this gene in the *Fbxw7* null cells. This is particularly surprising as *Ccnd1* is also a target of c-Myc and E2F [26,27]. Thus, not all target genes in a particular pathway are activated upon *Fbxw7* loss. This may be due to differences in the dosage level of each substrate following *Fbxw7* deletion, or alternative pathways may prevent changes in downstream target genes.

We did observe some cell-to-cell heterogeneity in substrate accumulation in our tumor staining (Fig. 4). Consistent with this, some genes displayed a prominent bimodal distribution in mRNA levels (*Vim*, *Cdkn2d*, *Brca1, Hk2*, *Cdk6, Cdc25A*, *Ccnd1*, *Snai2*; Marked by arrows in Fig. 5B-E), suggesting that cell-to-cell variation occurs in nontumor cells as well. However, *Fbxw7* loss resulted in mostly uniform, whole-population shifts in gene expression. Minimal differences from Fig. 5 were observed if individual cells were stratified into ``high'' and ``low'' expressing cells based on median gene expression, confirming that the observed changes were relatively uniform (data not shown).

Collectively, these data suggest that gene dysregulation in response to *Fbxw7* loss occurs prior to tumor development, and that genes in the c-Myc and E2F pathways are predominantly affected. Several of the Notch1-ICD targets we assayed were also influenced by *Fbxw7* loss, while deregulation of the c-Jun pathway as a whole was not strongly impacted. These data indicate that altered regulation of the E2F and c-Myc pathways may be critical first steps to mammary tumor development following *Fbxw7* loss.

E2F and c-Myc pathway dysregulation dominate in Fbxw7$^{-/-}$ *mammary tumors*

We next hypothesized that dysregulation of Fbw7 substrates would induce broad transcriptome changes consistent with increased proliferation. To address this, we performed unbiased bulk RNA sequencing on non-cancerous, purified epithelial cell populations, WT mammary glands, and tumor samples. Compared to the changes in gene expression observed between WT gland and tumor samples, fewer changes in the gene expression profiles were observed between the non-cancerous *Fbxw7*$^{+/+}$ and *Fbxw7*$^{-/-}$ epithelial populations (Fig. 6A, nontumor epithelials), although 559 genes were significantly differentially expressed between the two groups (at least 2-fold change, p-val adj <0.05). Differential expression (DE) analysis revealed the upregulation of a multitude of cell cycle related genes, many of which are well-described E2F or c-Myc targets, including *Cdk6*, *Cdk1*, *Cdca3*, *Cdc20*, *Ccna2*, *Ccnb1*, *Cdk2*, and *Cdc6*. These genes were all upregulated approximately 2.5–4 fold upon *Fbxw7* deletion. We also observed a 3–4 fold suppression of the cell cycle inhibitor genes *Cdkn2c* and *Cdkn1c* in the *Fbxw7* null cells. This reinforces our single cell qPCR data indicating that, even prior to cancer development, loss of *Fbxw7* promotes high level expression of cell cycle genes, driving proliferation in epithelial cells.

To identify additional dysregulated pathways in an unbiased fashion, we performed gene set enrichment analysis (GSEA) with the MSigDB Hallmarks genesets using a cutoff of $p < 0.01$ and a false discovery rate (FDR) of <25% and found an enrichment of genesets involved in proliferation. Consistent with our DE analysis, E2F and c-Myc targets were strongly enriched in *Fbxw7*$^{-/-}$ vs. *Fbxw7*$^{+/+}$ non-cancerous epithelial cell populations, as were G2/M checkpoint and DNA repair genes (Fig. 6B left panels and Supplementary Fig. 2A). This again is consistent with

deregulation of the cell cycle being an early, critical first step prior to tumor development following *Fbxw7* loss. We did not observe a significant enrichment in c-Jun target genesets, consistent with our single cell data. While we were able to observe changes in a subset of Notch gene targets (*Heyl*, *Hes1*, *Notch3*, *Fzd1*, *Aph1a*, and *Rbx1*), the GSEA Notch geneset was not large enough for significance to be reached. Both our single cell and RNAseq studies are consistent with early dysregulation of the E2F and c-Myc pathways driving proliferation prior to breast tumor development.

As expected, much more variability was observed when comparing the transcriptional profiles of the WT mammary gland and tumor samples, indicating that gene expression becomes further dysregulated upon tumor formation (Fig. 6A, WT glands and tumors). We found that 3304 genes were significantly differentially expressed in tumor vs. WT mammary gland samples, implying that transformation results in additional changes that more broadly disrupt the transcriptome. However, DE seq analysis revealed the continued deregulation of several cell cycle genes seen after early *Fbxw7* loss, including *Cdk1*, *Cdca3*, *Cdc20*, *Ccna2*, *Ccnb1*, *Cdc6*, and *Cdkn2c* as well as additional cell cycle genes such as *Ccnb2*, *Cdkn2a*, and *Ccnd1*. We next performed unbiased GSEA on WT glands vs. $Fbxw7^{-/-}$ tumors to identify pathways associated with transformation. Similar to the late-pregnancy $Fbxw7^{-/-}$ epithelial cells, we found an enrichment of E2F and c-Myc targets, DNA repair, and G2/M checkpoint genes in our tumor samples, with an increase in normalized enrichment score (NES) vs. that observed in the nontumor epithelial cell comparison (Fig. 6B right panels and Supplementary Fig. 2B). The increase in the NES scores implies that the early gene expression changes observed in epithelial cells following loss of *Fbxw7* are reinforced as tumors develop. We also saw an enrichment of mitotic spindle genes, many of which are E2F target genes (Supplementary Fig. 2B). The mitotic spindle geneset was not significantly enriched in our non-tumor $Fbxw7^{-/-}$ epithelials, suggesting that long-term *Fbxw7* loss impacts cell division and chromosome stability through E2F upregulation.

Because the mammary gland contains a mixture of stromal and epithelial cells, while the tumor body is predominated by epithelials, we also performed unbiased GSEA analysis comparing WT purified epithelials vs. tumor samples. We again observed a significant enrichment of the E2F, c-Myc, DNA repair, and G2M pathways in the tumor samples, with an increase in NES for E2F pathway genes (Supplementary Fig. 2C) compared to that observed for $Fbxw7^{-/-}$ vs. $Fbxw7^{+/+}$ epithelials. We did not observe an increase in the NES over that for $Fbxw7^{-/-}$ vs. $Fbxw7^{+/+}$ epithelials in the c-Myc, DNA repair, or G2M pathways with this comparison, however these pathways remained significantly enriched. We also performed GSEA comparing $Fbxw7^{-/-}$ epithelial cells and tumor samples and again observed an enrichment of the E2F pathway in the tumors (Supplementary Fig. 2D), confirming the increase in E2F pathway dysregulation from early *Fbxw7* loss to tumor formation. Based upon our data, a clear progression in gene expression changes can be seen.

We next hypothesized that the $Fbxw7^{-/-}$-derived tumors would show a stronger enrichment in E2F and c-Myc pathways than other well-established mammary tumor models. To address this, we turned to the MMTV-PyMT breast tumor model. This model undergoes progressive breast cancer development, starting with hyperplasia at 6 weeks of age, neoplasia at 8, and carcinoma at 12 [19]. Similar to our study, Cai et al. observed that genes in the c-Myc, E2F, mitotic spindle, and G2M checkpoint pathways were upregulated early (8 weeks) and remained upregulated at the carcinoma stage [19]. We chose to compare gene expression in our tumors with that of the 8 week (neoplasia) samples, as our tumors were likely at a similar developmental stage based on differentiation/morphology. While some similarities were observed, the two sample types exhibited overall different gene expression profiles (Fig. 6C). Unbiased GSEA analysis revealed a strong enrichment of c-Myc, E2F, and DNA repair targets in $Fbxw7^{-/-}$ tumors compared to the 8 week PyMT tumors (Supplemental Fig. 2E and data not shown). Thus, while enrichment of E2F and c-Myc targets were observed in the PyMT model, *Fbxw7* loss results in a stronger deregulation of these targets. In contrast, GSEA revealed an enrichment of angiogenesis and K-Ras-mediated signaling in the PyMT model in comparison to our model (data not shown). Our data suggest that while some similarities exist between the two models, the $Fbxw7^{-/-}$ model is mechanistically distinct from the MMTV-PyMT model. Upon *Fbxw7* loss, changes in cell cycle gene expression, prominently driven by E2F and c-Myc, occur early within the mammary epithelial cells. As breast tumors develop, E2F dysregulation continues, and signatures related to DNA repair, G2M checkpoint genes, and the mitotic spindle become apparent. Thus, while increased proliferation is a critical, early step in the transformation process, continued deregulation of DNA repair, G2/M checkpoint, and mitotic spindle genes likely facilitate tumorigenesis.

Fbxw7 loss triggers Trp53 mutation

Given the changes we observed over time in gene expression and the wide range in latency from early *Fbxw7* loss to tumor development, we hypothesized that perhaps a critical ``second-hit'' occurred which ultimately promoted tumor formation. One candidate for this second hit is *TP53*. Mutations in *TP53* occur in approximately 23% of all breast cancers, with about 70% of these being missense mutations [29]. Often, *TP53* mutation drives tumorigenesis by inactivating p53's downstream tumor suppressive functions [29]. Such mutations have been shown to accelerate transformation in a range of tissues in combination with *FBXW7* loss/mutation or cyclin E dysregulation [30–33]. In breast cancer specifically, *TP53* mutation combined with overexpression of cyclin E accelerates tumorigenesis, implying genetic cooperation during transformation [6,34]. As such, we hypothesized there would be an enrichment for genetic alterations in both *FBXW7* and *TP53* in breast cancer patients. To test this hypothesis, we queried available breast cancer datasets using the cBioPortal (8874 patients from 15 studies) to determine the co-occurrence of *TP53* and *FBXW7* mutations. We found a statistically significant enrichment of *TP53* mutations in patients harboring an *FBXW7* mutation (78%) vs. those without (47%; Fig. 7A). While hormone receptor and *HER2* expression status were not annotated for the majority of these samples, we were able to examine the relationship between *FBXW7* and *TP53* mutations in 1257 ER+/*HER2*- samples, 307 ER-/*HER2*- samples, and 198 HER2+ samples (Supplementary Fig. 3). Regardless of the category examined, the association between *FBXW7* and *TP53* mutations was observed, suggesting that the subtype of breast cancer does not influence the relationship between *FBXW7* and *TP53* mutations (Supplementary Fig. 3). No difference in overall survival was observed between patients harboring a *FBXW7* single mutation and those with both *FBXW7* and *TP53* mutations in any category examined (data not shown). Although we were only able to use *FBXW7* mutational status and not overall expression level in these analyses, these data suggest that *TP53* mutations synergize with *FBXW7* mutations in human breast tumorigenesis.

Given this finding of an enrichment of *TP53* mutations, we hypothesized that *Trp*53 mutations would be found in our tumor samples. To test this hypothesis, we sequenced the most commonly mutated exons of *Trp53* (exons 5–8 which include the DNA binding domain; 29) observed in breast cancer patients in our murine tumor samples. Using WT mammary tissue and matched tail samples as controls, we identified somatic missense mutations in all (6/6) tumor samples analyzed (Fig. 7B, highlighted in red). We identified 19 different missense mutations, with 10 occurring in exons 5–6 and 9 in exons 7–8. In contrast, we found 6 WT *Trp53* alleles in exons 5–6, and 12 in exons 7–8, indicating that not every allele is mutated within the tumor tissue. The total percentage of mutated alleles sequenced was 51.3% vs. 48.7% WT alleles (Fig. 7C). We found 2 silent mutations in exons 5–6 and 9 in exons 7–

8, however silent mutations were also uncovered in WT mammary tissues or matched *Fbxw7*$^{fl/fl}$;LGB Cre+ tail tissues, suggesting they occur independently of *Fbxw7* excision. Each tumor exhibited a different mutational spectrum, with no codon being mutated in more than one tumor sample. All mutations, with the exception of V291L, occurred at amino acids conserved between human and mouse *p53* (Fig. 7B) and were observed in codons mutated in breast cancer patients ([35–37] and cBioPortal query). One mutation, G242S (G245S human), is defined as a hotspot conformational mutation in breast cancer and is found with an overall frequency of approximately 2.8% [37]. Interestingly, the exact same nucleotide change (GGC to AGC) observed here has been reported in patients, suggesting this represents a potential ``hot-spot'' for p53 inactivation in both species [36,37]. E284K has also been detected in several patient tumors [36]. While we were unable to determine if *Trp53* mutations are heterozygous or homozygous, we were able to identify multiple different mutations in the majority of our tumor samples, pointing to some intratumor heterogeneity. Only a single missense mutation was found per sequenced allele, with the exception of one allele in tumor 5 that harbored 3 different mutations (G242S, E284K, V291I). Collectively, these data indicate that loss of *Fbxw7* in tumors is associated with the acquisition of *Trp53* missense mutations.

To determine if loss of *Trp*53 occurred prior to tumor development, we analyzed nontumor epithelial cells from pregnant *Fbxw7*$^{-/-}$ mice and identified mutations in a subset (3/5) of the samples tested. Importantly, the number of mutated alleles identified in normal tissue was lower than that uncovered in the tumor samples, with 3 mutated and 14 WT *Trp53* alleles in exons 5–6. Similarly, we found 3 mutations and 9 WT alleles in exons 7–8, with one allele containing two separate mutations. In contrast to tumor tissues, the total percentage of mutated alleles in the nontumor samples was much lower (20.7% mutated vs. 79.3% WT, Fig. 7C). All mutations uncovered in nontumor samples were different from those in the tumor samples and are highlighted in green in Fig. 7B. These data suggest that *Trp53* mutations can be acquired early following *Fbxw7* loss, with additional mutations accumulating during tumorigenesis. Collectively, this implies that loss of *Tp*53 occurs early in the transformation process following loss of *Fbxw7*, but the mutational burden accelerates as tumors form.

Given that some *TP53* mutations can increase p53 protein stability [38], we examined p53 protein levels by IHC, but detected overexpression in only two tumors, with most showing low-moderate expression (Fig. 7D). Although neither of the mutations in these two tumors have been previously linked to p53 mislocalization, p53 was at least partially localized to the cytoplasm in these samples, suggesting they may interfere with proper p53 function (Fig. 7D). We were unable to detect increased expression of p53 in tissues from pregnant, non-tumor bearing mice (data not shown). The detection of *Trp53* mutations early after *Fbxw7* loss and the accumulation of additional mutations upon tumorigenesis strongly suggests that *Fbxw7* loss and *Trp53* missense mutations genetically cooperate to promote breast tumorigenesis. The enrichment of *TP53* mutations in *FBXW7* mutant patient-derived tumors suggests the same synergy between these two pathways is critical in humans as well.

Discussion

Fbw7 has a well-known role in regulating the expression levels of a multitude of transcription factors that control cell proliferation and survival pathways and can exhibit tissue-specific effects on its substrates and their respective downstream activities. For instance, in embryonic stem cells, *Fbxw7* knockdown affects only c-Myc abundance while other substrates are unaffected [39]. Additionally, ablation of Fbw7 in the brain primarily induces Notch and c-Jun accumulation, while other substrates are unchanged [40]. The effect of *Fbxw7* loss on tumorigenesis has been studied in several cancer types [10,13,30,32,33], however *Fbxw7* loss is not always sufficient for tumorigenesis [33,41] and the contribution of *Fbxw7* loss to breast tumorigenesis has not been studied. Here, we determine that loss of *Fbxw7* serves as an initiating event in the induction of breast tumor development in a murine model system. A proposed mechanism is depicted in Fig. 7E. Our data suggest that the E2F and c-Myc pathways are affected early after *Fbxw7* loss and remain dysregulated following tumor formation. We suggest that persistent cell cycling in the presence of DNA damage results in tumorigenesis. Additionally, the loss of *Fbxw7* triggers the acquisition of *Trp53* mutations in mouse mammary tumors, suggesting that *Fbxw7*/*Trp53* alterations cooperate during transformation. Importantly, an enrichment of *TP53* mutations in *FBXW7*-altered breast cancer samples indicates this genetic cooperativity also occurs in humans.

How might dysregulated levels of c-Myc and cyclin E drive tumorigenesis? The role of c-Myc in oncogenesis is well-known, as it acts as both a driver of both proliferation and apoptosis [26,42]. Normally c-Myc is expressed at a low, constitutive level in dividing cells, and removal of growth factor signaling results in its degradation [26,42]. In our study, *Fbxw7* loss resulted in sustained c-Myc overexpression, which is known to promote proliferation through the up-regulation of cell cycle genes [26]. Consistent with this, we observed the upreguation of c-Myc-regulated cell cycle genes such as *Ccna2*, *Cdk6*, and *Cdk4* in our single cell qPCR and/or bulk RNAseq following *Fbxw7* loss (Fig. 5C and 6B). However, high levels of c-Myc can also trigger apoptosis. We were able to observe the upregulation of several pro-apoptotic factors in our bulk RNA-seq data following *Fbxw7* loss, including *Bcl2l11*, *Bcl2l14*, *Bcl10*, *Bcl2l1*, and *Bnipl*. We also observed suppression of the anti-apoptotic factor *Bcl2*, which is known to be repressed by c-Myc and cyclin E [43]. Consistent with both the pro-proliferative and anti-apoptotic effects of c-Myc, we observed increased proliferation and apoptosis in our tumors as evidenced by Ki67 and cleaved caspase-3 staining, respectively. Interestingly, c-Myc can induce apoptosis by inducing p53 expression and activation [44]. Thus, a loss of p53 function would shift the balance between proliferation and apoptosis. We hypothesize that the acquisition of *TP53* mutations contributes to breast tumorigenesis in *FBXW7*-altered patients by preventing high levels of c-Myc from promoting apoptosis. Consistent with this hypothesis, B-cell lymphomas induced by c-Myc overexpression lost WT *TP53* during tumor development [44]. Additional experiments to delineate the interplay between *Trp53* and *Fbxw7* mutation-induced c-Myc overexpression in breast cancer will be needed to directly test this hypothesis.

The relationship between cyclin E and Fbw7 in cancer has also been well-studied. Normally, cyclin E levels are strictly regulated during the cell cycle, with Fbw7 mediating cyclin E degradation during S phase [25]. During G1 phase, cyclin E-Cdk2 phosphorylates Rb protein, relieving its inhibition of the E2F1, E2F2, E2F3, and E2F4 transcription factors to promote the expression of genes regulating S phase initiation and progression [27,45]. We observed a prominent upregulation of cell cycle genes early after *Fbxw7* loss, which remained dysregulated in resulting breast tumors. As many of these genes are known to be direct targets of E2F, this strongly suggests that loss of *Fbxw7* triggers hyperplasia through E2F deregulation, resulting in tumorigenesis. Additionally, similar to c-Myc, E2F can promote the expression of pro-apoptotic genes [27], consistent with the increase in cleaved caspase 3 staining observed in our tumors. Cai et al. also observed early dysregulation of the E2F pathway in the MMTV-PyMT tumor model [19]. While E2F targets were more strongly dysregulated in our *Fbxw7*$^{-/-}$ model, the dysregulation of E2F in multiple models suggests that E2F pathway disruption is a key contributor to breast tumor development [19]. Importantly, we cannot exclude that family

members other than the Rb-regulated E2Fs are also playing a role in the observed hyperplasia following loss of *Fbxw7*. Our RNAseq shows enriched expression of DNA repair, mitotic spindle, and G2/M checkpoint genes in the *Fbxw7*$^{-/-}$ tumors, in line with deregulation of E2F transcriptional activity. It should be emphasized that significant crosstalk exists between the c-Myc and E2F pathways [46,47]. Thus, these pathways likely continually reinforce one another in the absence of *Fbxw7*. Additional experiments will be required to precisely define the unique and overlapping molecular targets resulting from c-Myc and E2F dysregulation.

In contrast to a clear upregulation of E2F and c-Myc target genes early after *Fbxw7* loss and upon tumor formation, we found little effect of *Fbxw7* loss on c-Jun/AP-1 target genes in any of our analyses, despite a high expression of c-Jun itself. c-Jun is more predominantly expressed in human breast cancers vs. normal tissue, however its expression has been observed mainly at the leading edge of tumors and has been associated with increased invasiveness and angiogenesis [48,49]. Consistent with this finding, the tumors that formed from *Fbxw7* loss in our model system were noninvasive and moderately to well-differentiated, suggesting that alterations in c-Jun may be more relevant to the transition from a more- to less-differentiated and/or aggressive tumor type. In addition, we did not uncover strong effects on Notch1-ICD signaling in our tumor samples, although early dysregulation of Notch1-ICD likely contributes to the lactation and involution defects in our *Fbxw7*$^{-/-}$ mice, as both phenotypes have been observed with sustained Notch1-ICD overexpression [23]. Hu et al. also observed that a small number of their MMTV/Notch1-ICD transgenic animals developed hyperplasia [23]. Thus, early Notch1-ICD dysregulation following *Fbxw7* loss may also contribute to over-proliferation.

It is notable that *Fbxw7* loss promoted *Trp53* mutation in our breast cancer study. Several studies have reported a relationship between *FBXW7* loss and *TP53* mutation in other cancers. For instance, co-deletion or mutation of *TP53* in the absence of one or more alleles of *FBXW7* has been shown to drive T-ALL, intestinal adenomas, and epithelial tumors in response to ionizing radiation [9]. *Fbxw7/Pten*$^{-/-}$ uterine carcinosarcomas also accumulate *Trp53* mutations [33]. The discovery of *Trp53* mutations soon after *Fbxw7* deletion in our model suggests that the two cooperate in breast cancer as well. Importantly, our studies mechanistically link *Fbxw7* loss with the development of *Trp*53 mutations in breast tumorigenesis. As p53 plays a critical role in promoting apoptosis in response to DNA damage and cell stress, loss of p53 function through mutation would facilitate tumorigenesis driven by E2F and c-Myc-enforced cell cycling. Consistent with this notion, p53 activity has been shown to restrain the effects of elevated cyclin E on genomic instability in the absence of *Fbxw7* [50]. p53 loss also allows for E2F1-induced S phase entry through suppression of the G1 checkpoint [51]. It is therefore likely that decreased *Fbxw7* expression results in a selective pressure for the acquisition of *Trp53* loss of function mutations through its effects on cyclin E and E2F.

The *Fbxw7*$^{-/-}$ tumors that developed most closely resemble the human breast cancer luminal B subtype, as they are ERα+, PR-, and exhibit high Ki67 staining. While ERα+ human breast cancers are not as frequently mutated for *TP53* compared to basal-like or HER2-enriched tumors, *TP53* mutations do occur in approximately 25% of luminal B cancers [52]. Consistent with our results, luminal B cancers have a higher proportion of missense mutations in the DNA binding domain of *TP53* compared to other subtypes [52]. Further, Silwal-Pandit showed that *TP53* mutations are predictive of reduced survival only in ERα+ disease [52]. Collectively, this suggests that the accumulation of *TP53* missense mutations that are triggered by *FBXW7* loss are likely to contribute to disease progression.

Conclusions

In conclusion, our results have clear implications for understanding breast cancer initiation, in which loss of *FBXW7* expression is relatively common. *Fbxw7* loss in the mouse mammary gland initiates tumor development, with the tumors subsequently accumulating mutations within *Trp53*. Significant changes to gene expression were detectable soon after *Fbxw7* loss, even before tumor formation occurred. Our data suggest that targeting the c-Myc and cyclin E-E2F pathways, for example through synthetic lethal approaches or Cdk2 inhibition, may be particularly helpful in the treatment of patients with tumors characterized by diminished *FBXW7* expression. Given the well-known roles of p53 in tumor suppression and the clear connection between *FBXW7*, *TP53* status, and luminal B-type breast cancers, our study further supports the ongoing search for new therapeutic strategies to target *TP53*-mutant cancers [53].

Data availability

All RNAseq data are available in GEO Omnibus #GSE144690, https://www.ncbi.nlm.nih.gov/geo/query/acc.cgi?acc=GSE144690.

Funding sources

This work was supported in part by funding from Midwest Athletes against Childhood Cancer and the NIH (CA204231) to SR and an American Cancer Society Research Scholar Grant (22511-RSG-12-132-01-CCG) to ACM. Additional research support to S. Rao provided by a charitable gift from Ms. Nanette Gardetto.

Declaration of Competing Interest

The authors declare that they have no known competing financial interests or personal relationships that could have appeared to influence the work reported in this paper.

Acknowledgments

The authors would like to Scott Wood for technical support, Benedetta Bonacci for assistance with flow cytometry, Barbara Fleming for histology, and Bruce E. Clurman for the gift of the anti-Fbw7 antibody.

Appendix A. Supplementary data

Supplementary data to this article can be found online at https://doi.org/10.1016/j.neo.2020.07.001.

References

1. Shimizu K, Nihira NT, Inuzuka H, Wei W. Physiological functions of FBW7 in cancer and metabolism. *Cell Signal* 2018;**46**:15–22.
2. Spruck CH, Won KA, Reed SI. Deregulated cyclin E induces chromosome instability. *Nature* 1999;**401**:297–300.
3. Ekholm-Reed S, Spruck CH, Sangfelt O, van Drogen F, Mueller-Holzner E, Widschwendter M, Zetterberg A, Reed SI, Reed SE. Mutation of hCDC4 leads to cell cycle deregulation of cyclin E in cancer. *Cancer Res* 2004;**64**:795–800.
4. Loeb KR, Kostner H, Firpo E, Norwood TD, Tsuchiya K, Clurman BE, Roberts JM. A mouse model for cyclin E-dependent genetic instability and tumorigenesis. *Cancer Cell* 2005;**8**:35–47.
5. Bortner DM, Rosenberg MP. Induction of mammary gland hyperplasia and carcinomas in transgenic mice expressing human cyclin E. *Mol Cell Biol* 1997;**17**:453–9.

6. Smith APL, Henze M, Lee JA, Osborn KG, Keck JM, Tedesco D, Bortner MP, Rosenberg MP, Reed SI. Deregulated cyclin E promotes p53 loss of heterozygosity and tumorigenesis in the mouse mammary gland. *Oncogene* 2006;**25**:7245–59.
7. Weng AP, Ferrando AA, Lee W, Morris IV JP, Silverman LB, Sanchez-Irizarry SC, Blacklow SC, Look AT, Aster JC. Activating mutations of NOTCH1 in human T cell acute lymphoblastic leukemia. *Science* 2004;**306**:269–71.
8. Bahram F, Von Der Lehr N, Cetinkaya C, Larsson LG. c-Myc hot spot mutations in lymphomas result in inefficient ubiquitination and decreased proteasome-mediated turnover. *Blood* 2000;**95**:2104–10.
9. Cao J, Ge M-H, Ling Z-Q. Fbxw7 tumor suppressor: a vital regulator contributes to human tumorigenesis. *Medicine (Baltimore)* 2016;**95** e2496.
10. Babaei-Jadidi R, Li N, Saadeddin A, Spencer-Dene B, Jandke A, Muhammad EE, Ibrahim EE, Muraleedharan R, Abuzinadah M, Davis H, Lewis A, Watson A, Behrens A, Tomlinson I, Nateri AS. FBXW7 influences murine intestinal homeostasis and cancer, targeting Notch, Jun, and DEK for degradation. *J Exp Med* 2011;**208**:295–312.
11. Wei W, Jin J, Schlisio S, Harper JW, Kaelin WG. The v-Jun point mutation allows c-Jun to escape GSK3-dependent recognition and destruction by the Fbw7 ubiquitin ligase. *Cancer Cell* 2005;**8**:25–33.
12. Gregory MA, Hann SR. c-Myc proteolysis by the ubiquitin-proteasome pathway: stabilization of c-Myc in Burkitt's lymphoma cells. *Mol Cell Biol* 2000;**20**:2423–35.
13. Akhoondi S, Sun D, Von Der Lehr N, Apostolidou S, Klotz K, Maljukova A, Cepeda D, Fiegl H, Dofou D, Marth C, Mueller-Holzner E, Corcoran M, Dagnell M, Nejad SZ, Nayer BN, Zali MR, Hansson J, Egyhazi S, Petersson F, Sangfelt P, Nordgren H, Grander D, Reed SI, Widschwendter M, Sangfelt O, Spruck C. FBXW7/hCDC4 is a general tumor suppressor in human cancer. *Cancer Res* 2007;**67**:9006–12.
14. Akhoondi S, LindstrÎm L, Widschwendter M, Corcoran M, Bergh J, Spruck C, GrandÅr D, Sangfelt O. Inactivation of FBXW7/hCDC4-β expression by promoter hypermethylation is associated with favorable prognosis in primary breast cancer. *Breast Cancer Res* 2010;**12**:R105.
15. Ibusuki M, Yamamoto Y, Shinriki S, Ando Y, Iwase H. Reduced expression of ubiquitin ligase FBXW7 mRNA is associated with poor prognosis in breast cancer patients. *Cancer Sci* 2011;**102**:439–45.
16. Thompson BJ, Jankovic V, Gao J, Buonamici S, Vest A, Lee JM, Zavadil J, Nimer SD, Aifantis I. Control of hematopoietic stem cell quiescence by the E3 ubiquitin ligase Fbw7. *J Exp Med* 2008;**205**:1395–408.
17. Selbert S, Bentley DJ, Melton DW, Rannie D, Lourenμo P, Watson CJ, Clarke AR. Efficient BLG-Cre mediated gene deletion in the mammary gland. *Transgenic Res* 1998;**7**:387–96.
18. Grim JE, Gustafson MP, Hirata RK, Hagar AC, Swanger J, Welcker M, Hwang HC, Ericsson J, Russell DW, Clurman BE. Isoform- and cell cycle-dependent substrate degradation by the Fbw7 ubiquitin ligase. *J Cell Biol* 2008;**181**:913–20.
19. Cai Y, Nogales-Cadenas R, Zhang Q, Lin JR, Zhang W, O'Brien K, Montagna ZD, Zhang ZD. Transcriptomic dynamics of breast cancer progression in the MMTV-PyMT mouse model. *BMC Genomics* 2017;**18**:1–14.
20. Singh S, Kumar S, Srivastava RK, Nandi A, Thacker G, Murali H, Kim S, Baldeon M, Tobias J, Blanco MA, Saffie R, Zaidi MR, Sinha S, Busino L, Fuchs SY, Chakrabarti R. Loss of ELF5–FBXW7 stabilizes IFNGR1 to promote the growth and metastasis of triple-negative breast cancer through interferon-γ signalling. *Nat Cell Biol* 2020;**22**:591–602.
21. Balamurugan K, Mendoza-Villanueva D, Sharan S, Summers GH, Dobrolecki MT, Lewis MT, Sterneck E. C/EBPδ links IL-6 and HIF-1 signaling to promote breast cancer stem cell-associated phenotypes. *Oncogene* 2019;**38**:3765–80.
22. Rustighi A, Zannini A, Tiberi L, Sommaggio R, Piazza S, Sorrentino G, Nuzzo A, Tuscano A, Eterno V, Benvenuti F, Santarpia L, Aifantis I, Rosato A, Bicciato S, Zambelli A, Del Sal G. Prolyl-isomerase Pin1 controls normal and cancer stem cells of the breast. *EMBO Mol Med* 2014;**6**:99–119.
23. Hu C, DiÅvart A, Lupien M, Calvo E, Tremblay G, Jolicoeur P. Overexpression of activated murine Notch1 and Notch3 in transgenic mice blocks mammary gland development and induces mammary tumors. *Am J Pathol* 2006;**168**:973–90.
24. Blakely CM, Sintasath L, D'Cruz CM, Hahn KT, Dugan KD, Belka GK, Chodosh LA. Developmental stage determines the effects of MYC in the mammary epithelium. *Development* 2005;**132**:1147–60.
25. Minella AC, Loeb KR, Knecht A, Welcker M, Varnum-Finney BJ, Bernstein JM, Roberts JM, Clurman BE. Cyclin E phosphorylation regulates cell proliferation in hematopoietic and epithelial lineages in vivo. *Genes Dev* 2008;**22**:1677–89.
26. Bretones G, Delgado MD, LeÆn J. Myc and cell cycle control. *Biochim Biophys Acta – Gene Regul Mech* 2015;**1849**:506–16.
27. Bracken AP, Ciro M, Cocito A, Helin K. E2F target genes: unraveling the biology. *Trends Biochem Sci* 2004;**29**:409–17.
28. Lee M-Y, Moreno CS, Saavedra HI. E2F activators signal and maintain centrosome amplification in breast cancer cells. *Mol Cell Biol* 2014;**34**:2581–99
29. Walerych D, Napoli M, Collavin L, Del Sal G. The rebel angel: mutant p53 as the driving oncogene in breast cancer. *Carcinogenesis* 2012;**33**:2007–17.
30. Mao JH, Perez-Losada J, Wu D, DelRosario R, Tsunematsu R, Nakayama KI, Brown K, Bryson S, Balmain A. Fbxw7/Cdc4 is a p53-dependent, haploinsufficient tumour suppressor gene. *Nature* 2004;**432**:775–9.
31. Grim JE, Knoblaugh SE, Guthrie KA, Hagar A, Swanger J, Hespelt J, Delrow T, Small T, Grady WM, Nakayama KI, Clurman BE. Fbw7 and p53 cooperatively suppress advanced and chromosomally unstable intestinal cancer. *Mol Cell Biol* 2012;**32**:2160–7.
32. Siu KT, Xu Y, Swartz KL, Bhattacharyya M, Gurbuxani S, Hua Y, Minella AC. Chromosome instability underlies hematopoietic stem cell dysfunction and lymphoid neoplasia associated with impaired Fbw7-mediated cyclin E regulation. *Mol Cell Biol* 2014;**34**:3244–58.
33. Cuevas IC, Sahoo SS, Kumar A, Zhang H, Westcott J, Aguilar M, Cortez JD, Sullivan SA, Xing C, Neil Hayes D, Brekken RA, Bae-Jump VL, Castrillon DH. Fbxw7 is a driver of uterine carcinosarcoma by promoting epithelial-mesenchymal transition. *Proc Natl Acad Sci USA* 2019;**116**:25880–90.
34. Lindahl T, Landberg G, Ahlgren J, Nordgren H, Norberg T, Klaar S, Holmberg L, Bergh J. Overexpression of cyclin E protein is associated with specific mutation types in the p53 gene and poor survival in human breast cancer. *Carcinogenesis* 2004;**25**:375–80.
35. Coles C, Condie A, Chetty U, Steel CM, Evans HJ, Prosser J. p53 mutations in breast cancer. *Cancer Res* 1992;**52**:5291–8.
36. Lai H, Lin L, Nadji M, Lai S, Trapido E, Meng L. Mutations in the p53 tumor suppressor gene and early onset breast cancer. *Cancer Biol Ther* 2002;**1**:31–6.
37. Freed-Pastor WA, Prives C. Mutant p53: One name, many proteins. *Genes Dev* 2012;**26**:1268–86.
38. Frum RA, Grossman SR. Mechanisms of mutant p53 stabilization in cancer. *Subcell Biochem* 2014;**85**:187–97.
39. Buckley SM, Aranda-Orgilles B, Strikoudis A, Apostolou E, Loizou E, Moran-Crusio K, Farnsworth CL, Koller AA, Dasgupta R, Silva JC, Stadtfeld M, Hochedlinger K, Chen EI, Aifantis I. Regulation of pluripotency and cellular reprogramming by the ubiquitin-proteasome system. *Cell Stem Cell* 2012;**11**:783–98.
40. Hoeck JD, Jandke A, Blake SM, Nye E, Spencer-Dene B, Brandner S, Behrens A. Fbw7 controls neural stem cell differentiation and progenitor apoptosis via Notch and c-Jun. *Nat Neurosci* 2010;**13**:1365–72.
41. Sancho R, Jandke A, Davis H, Diefenbacher ME, Tomlinson I, Behrens A. F-box and WD repeat domain-containing 7 regulates intestinal cell lineage commitment and is a haploinsufficient tumor suppressor. *Gastroenterology* 2010;**139**:929–41.
42. Hanson KD, Shichiri M, Follansbee MR, Sedivy JM. Effects of c-myc expression on cell cycle progression. *Mol Cell Biol* 1994;**14**:5748–55.
43. Eischen CM, Packham G, Nip J, Fee BE, Hiebert SW, Zambetti GP, Cleveland JL. Bcl-2 is an apoptotic target suppressed by both c-Myc and E2F–1. *Oncogene* 2001;**20**:6983–93.
44. Hemann MT, Bric A, Teruya-Feldstein J, Herbst A, Nilsson JA, Cordon-Cardo C, Cleveland JL, Tansey WP, Lowe SW. Evasion of the p53 tumour surveillance network by tumour-derived MYC mutants. *Nature* 2005;**436**:807–11.
45. Kent LN, Leone G. The broken cycle: E2F dysfunction in cancer. *Nat Rev Cancer* 2019;**19**:326–38.
46. Mudryj M, Hiebert SW, Nevins JR. A role for the adenovirus inducible E2F transcription factor in a proliferation dependent signal transduction pathway. *EMBO J* 1990;**9**:2179–84.
47. Leone G, Sears R, Huang E, Rempel R, Nuckolls F, Park CH, Giangrande P, Wu L, Saavedra HI, Field SJ, Thompson MA, Yang H, Fujiwara Y, Greenberg S, Orkin S, Smith C, Nevins JR. Myc requires distinct E2F activities to induce S phase and apoptosis. *Mol Cell* 2001;**8**:105–13.

48. Vleugel MM, Greijer AE, Bos R, van der Wall E, van Diest PJ. c-Jun activation is associated with proliferation and angiogenesis in invasive breast cancer. *Hum Pathol* 2006;**37**:668–74.
49. Jiao X, Katiyar S, Willmarth NE, Liu M, Ma X, Flomenberg N, Lisanti MP, Pestell RG. c-Jun induces mammary epithelial cellular invasion and breast cancer stem cell expansion. *J Biol Chem* 2010;**285**:8218–26.
50. Minella AC, Grim JE, Welcker M, Clurman BE. p53 and SCFFbw7 cooperatively restrain cyclin E-associated genome instability. *Oncogene* 2007;**26**:6948–53.
51. Lomazzi M, Moroni MC, Jensen MR, Frittoli E, Helin K. Suppression of the p53- or pRB-mediated G1 checkpoint is required for E2F-induced S-phase entry. *Nat Genet* 2002;**31**:190–4.
52. Silwal-Pandit L, Vollan HKM, Chin SF, Rueda OM, McKinney S, Osako T, Quigley DA, Kristensen VN, Aparicio S, BÖrresen-Dale AL, Caldas C, LangerÖd A. TP53 mutation spectrum in breast cancer is subtype specific and has distinct prognostic relevance. *Clin Cancer Res* 2014;**20**:3569–80.
53. Blandino G, Di Agostino S. New therapeutic strategies to treat human cancers expressing mutant p53 proteins. *J Exp Clin Cancer Res* 2018;**37**:30.